Ocean Systems Engineering, *Vol. 5, No. 1 (2015) 1-19*
DOI: http://dx.doi.org/10.12989/ose.2015.5.1.001

Effect of water jetting parameters on the penetration behavior of jack-up spudcan in surficial sand condition

Dong-Seop Han[1], Seung-Jun Kim[2] and Moo-Hyun Kim[*2]

[1]*Research Institute of Green Energy Equipment, Dong-A University, Busan, South Korea*
[2]*Coastal and Ocean Eng. Division, Zachry Dept. of Civil Eng., Texas A&M University, College Station, Texas, USA*

(Received December 20, 2014, Revised February 17, 2015, Accepted February 20, 2015)

Abstract. The water jetting system for a jack-up spudcan requires the suitable design considering the platform/spudcan particulars, environments, and soil conditions, either the surficial clay or surficial sand. The usage of water jetting depends critically on soil conditions. The water jetting is usually used for the smooth and fast extraction of the spudcan in the surficial clay condition. It is also required for inserting spudcan up to the required depth in the surficial sand condition, which is investigated in this paper. Especially, it should be very careful to use the water jetting during an installation of spudcan in the surficial sand condition, because there is a risk of overturning accident related to the punch-through. Therefore, in this study, the effect of water jetting flow rate and time on the change of soil properties and penetration resistance is analyzed to better understand their interactions and correlations when inserting the spudcan with water jetting in surficial sand condition. For the investigation, a wind turbine installation jack-up rig (WTIJ) is selected as the target platform and the multi layered soil (surficial sand overlaying clays) is considered as the soil condition. The environmental loading and soil-structure interaction (SSI) analysis are performed by using CHARM3D and ANSYS. This kind of investigation and simulation is needed to decide the proper water jetting flow rate and time of spudcan for the given design condition.

Keywords: jack-up platform; spudcan; water jetting; flow rate; duration; soil-structure interaction; surficial sand; soil resistance; punch-through

1. Introduction

Nowadays, the life-cycle of the 1st-generation jack-up rigs is almost over and many new jack-up rigs are to be built. Also, the demand of offshore wind turbine installation jack-up rigs is steadily increased. The spudcan is attached at the bottom of jack-up legs and used for temporarily fixing a jack-up platform on seabed. It may have the water jetting system for the smooth and fast installation and extraction operation, which requires the suitable design considering the platform size, shape of spudcan, soil, and environmental conditions. During the installation operation and extraction processes, if there is not enough resistance force and moment by soil, it can lead to the overturning accidents. To prevent this kind of accident, a spudcan should be inserted up to sufficient depth so that the whole structure can be supported by the sufficient resistance of soil

*Corresponding author, Professor, E-mail: m-kim3@tamu.edu

http://www.techno-press.org/?journal=ose&subpage=7 ISSN: 2093-6702 (Print), 2093-677X (Online)

(e.g., DNV codes 2012). On the other hand, the speed up of lowering and extracting processes is also important to reduce the operational cost.

The soil condition of seabed is largely categorized into the surficial clay and the surficial sand conditions with multiple layers of similar or other soils below it. The usage of water jetting is different depending on the soil conditions. The water jetting is used for the smooth and fast extraction of the spudcan mostly in the surficial clay condition because the spudcan is deeply inserted until the sufficient resistance of soil is reached. However, inserting the spudcan up to the required depth in the surficial sand condition is not so easy because the spudcan usually can't penetrate deeply into the sand layer. Many studies on the use of water jetting for the clay layer during the extraction process have been conducted, but studies on the use of water jetting for the sand layer during the penetration are still very rare (Han *et al*. 2014, Zhao *et al*. 2011, Qiu *et al*. 2012).

The penetration depth of a spudcan at the sand layer can be increased by water jetting, but simultaneously, the overturning resistance can be reduced and the punch-through failure can occur if water jetting flow rate and time are too excessive. So, the water jetting should be used spudcanvery carefully for the surficial sand condition. Therefore, in this study, in order to insert the spudcan up to the required depth of surficial sand, the effect of the water jetting, primarily the flow rate and time, on the change of soil properties and penetration resistance is analyzed. The simulation results can be used to develop a reasonable water-jetting strategy for the given situation.

For the investigation, a wind turbine installation jack-up rig (WTIJ) is selected as the target platform and the Gulf of Mexico (GoM) as the target site. The irregular wind and wave, and steady current recommended in API codes (2007) are applied as the environmental conditions and the external forces and moments at the connecting point between the leg and spudcan are calculated by using Charm 3D (Kang *et al*. 2012 and Yang *et al*. 2011) and ABAQUS programs. Next, the radius of disturbed area and the equivalent internal friction angle of the sand layer according to water jetting flow rate and time are calculated. Lastly, multi layered (sand overlying clay) soil profile is applied as soil condition, and the soil-structure interaction (SSI) analysis is performed by using ANSYS (2012) to analyze the effect of water jetting flow rate and time on the reaction of soil. For this purpose, the three-kinds of water jetting flow rates (240 m^3/h, 360 m^3/h, 480 m^3/h) with six radii of disturbed zones (1.5 m, 2.5 m, 3.5 m, 4.5 m, 5.5 m, 6.5 m) are respectively adopted as the design parameters for the case study (Tho *et al*. 2012 and Yu *et al*. 2012).

2. Loading analysis

2.1 Target platform

A jack-up wind turbine installation vessel (WTIV) typically has 4~6 legs and is operated in water depth within 100 m. The WTIV selected here as the target platform has 6 legs and is operated in the water depth of 75 m. Fig. 1 shows the schematic view of the wind turbine installation vessel including 6 legs. The total vertical structural loading of it is about 440MN including the weight of cranes, storage and water-ballast tanks. The maximum static vertical force occurs on the spudcan attached in a right-rear leg and its magnitude is 80.35 MN. This is selected as the target spudcan.

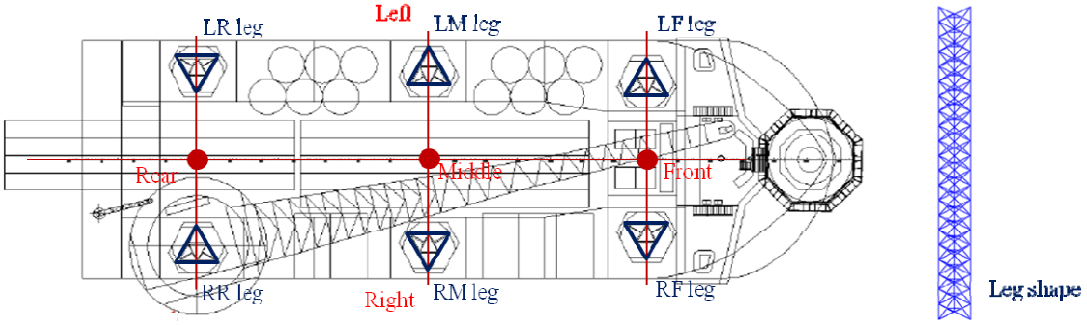

Fig. 1 Schematic of the jack-up wind turbine installation vessel (WTIV) and a leg

2.2 Environmental loadings

In order to simulate the structural behavior of the WTIV platform under the specific environmental condition, wind, wave, and current presented by API code were applied.

Wind Wind-velocity time-series can be generated based on the wind power spectrum presented by API wind spectrum, the spectral energy density ($s(f)$) at frequency (f) is described as below

$$S(f)=320\left(\frac{U_0}{10}\right)^2\left(\frac{z}{10}\right)^{0.45}\Big/\left(1+\tilde{f}^{\,n}\right)^{(5/3n)} \tag{1}$$

$$\tilde{f}=172f\left(\frac{z}{10}\right)^{2/3}\left(\frac{U_0}{10}\right)^{-0.75} \tag{2}$$

where n=0.468, z is the height above sea level, U_0 is the 1-hour mean wind speed at 10m above sea level. In this study, it is assumed that the platform is installed and operated at West region of GoM, so 39.9 m/s of 1-hour mean wind speed is considered as the 100-y return period wind. According to the general equation of wind force, the wind-force time series applied to the exposed surface (F_W) can be calculated as follows

$$F_W = CqS\sin\theta \tag{3}$$

where C is the shape coefficient (C=1.28 for flat plate), q is the wind pressure ($q=1/2\rho_a U^2_{T,z}$), ρ_a is the mass density of air, $U_{T,z}$ is the wind velocity at time (T) and at a height (z) above the mean sea level, S is the projected area of the member normal to the direction of the force, and θ is the angle between the direction of the wind and the axis of the exposed member or surface.

Wave & current For wave loading estimation, JONSWAP spectrum with peak enhancement factor =2.4 is used to simulate the time-series of irregular sea-surface elevations. As mentioned previously, it is assumed that the WTIV platform is installed and operated at West region of G.O.M. Table 1 shows the parameters applied to the wave spectrum (West G.O.M, 70 m mean sea level, 100y return period hurricane event), based on the API code. Also, according to the API code, current velocity at West G.O.M under 100y return period hurricane is 1.31 m/s uniformly applied up to 70.0 m depth.

Table 1 Parameters for simulation of wave elevation

Items	Values
Significant wave height(*m*)	11.2
Peak period(*s*)	15.1
Enhancement factor	2.4

For the normal component (q_n) of the distributed external force acting on the rod per unit length, the following equation is used based on the equation of generalized Morison equation

$$q_n = C_I \rho A_e \dot{v}_n + C_D \tfrac{1}{2} \rho D_s |v_{nr}| v_{nr} + C_m \rho A_e \ddot{r}_n \tag{4}$$

where C_I, C_D, and C_m are inertia, drag, and added mass coefficients, and $\dot{v}_n$, v_{nr}, and $\ddot{r}_n$ are normal fluid acceleration, normal relative velocity, and normal structure acceleration, respectively. The symbols ρ, Ds and A_e in the equation are fluid density, local diameter, and outer cross sectional area, respectively (Kim and Chen 1994, Kim and Ran 1994).

Fig. 2 shows the wind-velocity and wave-amplitude spectra generated by CHARM3D program for API spectrum and JONSWAP spectrum. The respective time histories were first generated from the input theoretical spectra for time-domain simulations. The respective spectra were also regenerated from the time series and compared with the input spectra for double checking purpose.

Combination of wind, wave, and current loads The time-series of environmental loadings on all the members due to wave, wind, and current in 70 m mean water level were calculated by using the Charm3D program considering various cases such as peak wave, peak wind, and peak current cases in the operation and installation conditions. Table 2 shows the environmental forces on the spudcan in peak wave, peak wind, and peak current cases.

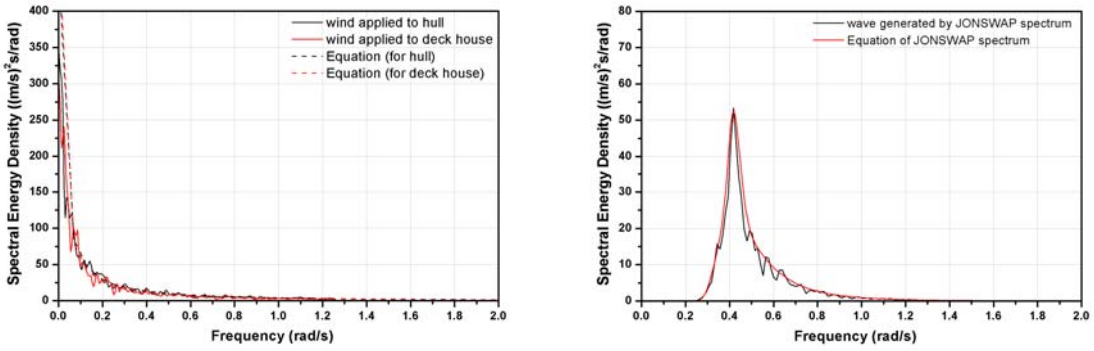

(a) wind energy density (b) wave energy density

Fig. 2 Comparison of wind and wave spectrum generated by CHARM3D program with API spectrum and JONSWAP spectrum

Table 2 The environmental forces applied on the spudcan in peak wave, peak wind, and peak current cases

Load cases	Forces (*kN*)			Moment (*MN-m*)
	Fx (Longitudinal)	Fy (Transverse)	Fz (Vertical)	Mx (Overturn)
Peak wind (wind/wave angle=15º)	344	1,701	-82	-66.7
Peak wave (wind/wave angle=15º)	474	2,777	-82	-103.1
Peak Current (wind/wave angle=0º)	3	1,480	-83	-50.1

In this study, the additional dynamic vertical loading (Fz) applied on the spudcan is only considered because the slope of the bottom plate is mainly related with the vertical loading during the lowering process. Accordingly, the required vertical reaction of soil is 80.45 MN when considering both structural weight (80.35 MN) and 1.2-times environmental loading (83 kN) i.e., the additional dynamic loading in the z direction is small compared to the weight of the structure. In an independent analysis, the resistance from the soil for the corresponding horizontal shear and over-turning moment is found to be sufficient if the submergence depth is greater than half of the spudcan height.

3. Water jetting effect

3.1 Water jetting theory

The detailed soil modeling and its interaction with structure are detailed in author's previous paper (Han *et al*. 2014) and the same theory/formulas are used here. Water jetting is frequently used to speed up the installation and extraction of the jack-up spudcan. When water jetting is operated, the pore pressure of the region near water nozzles is changed, and the changed pore pressure and the seepage force affect the effective vertical soil pressure. So, the shear strength of soil varies due to the change of the effective vertical pressure, as shown in Eq. (5). In other words, if the changes of the pore pressure and seepage force are theoretically estimated, the change of shear strength of soil can be determined. As for SSI analysis, the effect of the pore-pressure and seepage-force changes on the soil shear strength can be more simply considered by applying the equivalent internal friction angle, as suggested by Duan *et al*. (2013). Since other parameters, such as cohesion, friction coefficient, etc., also change due to the water jetting, the actual physics can be more complicated and the current model is a simplified one. However, our independent sensitivity study (Han *et al*. 2014) reveals that the sensitivity with other parameters is relatively less important. In this regard, to consider the change of shear strength of sand soil due to water jetting, the equivalent internal friction angles are calculated by the equations suggested by Duan *et al*. (2013). Then, they are subsequently applied to the material property of the sand models as requested by ANSYS for SSI analysis. The relation between the radius of disturbed zone $R(t)$ and jetting time t is.

$$t = t_0 + \frac{\pi\gamma_w^2 h}{q} + \frac{c_f n\gamma_w R(t)}{k\left(R(t)-R_w\right)}\left(\frac{R_w^2}{2}\ln\frac{R_w}{R(t)} + \frac{R(t)^2}{12}\right) \tag{5}$$

where t_0 is the initial jetting time, γ_w is the specific weight of water, h is the thickness of seepage layer, q is the jetting flow rate of a nozzle, c_f is the compressibility of the sand soil, n is current porosity, k is the permeability coefficient, R_w is the radius of a nozzle. The equivalent internal friction angle (φ') of the sand layer at jetting time t is expressed as below

$$\varphi' = \arctan\left(\frac{\sigma_n - u - f}{\sigma_n - u_0}\tan\varphi\right) \tag{6}$$

where σ_n is the overburden pressure

$$\sigma_n = u_0 + \frac{Q_f}{\pi D_o H\tan\varphi} \tag{7}$$

The symbol u is the pore pressure due to jetting time t and given by

$$u = u_0 + \frac{q\gamma_w R(t)}{2\pi kh\left(R(t)-R_w\right)}\left[\ln\frac{r}{R(t)} - \frac{r}{R(t)} + 1\right] \qquad R_w \le r \le R(t) \tag{8}$$

and f is the seepage force at jetting time t

$$f = -\frac{q\gamma_w R(t)}{2\pi kh\left(R(t)-R_w\right)}\left[\frac{1}{r} - \frac{1}{R(t)}\right] \tag{9}$$

where φ is the initial internal friction angle of the soil, u_0 is the initial pore pressure, Q_f is the bearing capacity of the soil, r is the distance between the *i-th* nozzle and point $M(r, \theta)$, D_o is the diameter of spudcan, H is the depth of the overlaid thin sand layer.

3.2 Effect of water jetting on the change of sand properties

Substituting the environmental conditions into Eqs. (5) and (6), the radius of disturbed zone ($R(t)$) and the equivalent internal friction angle (φ) due to water jetting can be estimated according to the water jetting time t. As shown in Fig. 4, the sand region is divided into many columns. Since the sand layer is shallow and the jetting direction is near vertical, the equivalent internal friction angle for each column is assumed to be the same. It is also assumed that the jetted water does not penetrate into the clay region. The values presented in Figs. 3(b) and 5 are the averaged values of the point with two neighboring points. Fig. 3 shows the corresponding jetting time to the radius of disturbed zone and the equivalent internal friction angle of sand layer below each jetting nozzle according to the water jetting flow rate. As shown in Fig. 3, the arrival time to the target radius due to the water jetting is reduced with increasing flow rate from 240 m^3/h to 480 m^3/h. For fixed flowrate, the time to reach the sequential target radius is increased quadratically, as expected. Whereas, the equivalent internal friction angle of soil at a point below the jetting nozzles is significantly reduced with increasing influenced radius and flow rate.

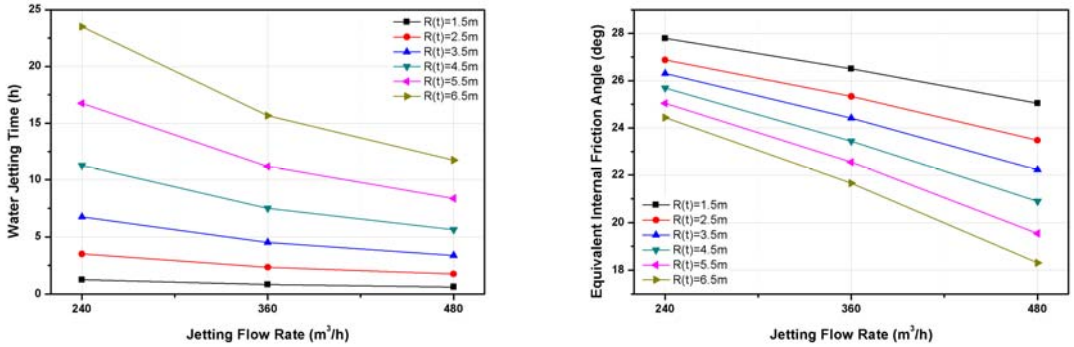

(a) water jetting time (b) equivalent internal friction angle

Fig. 3 Corresponding jetting time to the radius of disturbed zone and the equivalent internal friction angle of sand layer below each nozzle according to the water jetting flow rate (when k = 5E-5 m/s, R_w = 0.075 m)

Table 3 Equivalent internal friction angle of the sand layer along the radius of soil with respect to the radius of disturbed zone (q=240 m^3/h)

Model cases	1	2	3	4	5	6
Jetting time, t	1.25h	3.50h	6.75h	11.25h	16.75h	23.50h
Radius of disturbed zone, $R(t)$	1.5 m	2.5 m	3.5 m	4.5 m	5.5 m	6.5 m
Radius of wet sand, Rs	Equivalent internal friction angle, φ' (deg)					
0.5	30.0	30.0	30.0	30.0	29.8	29.2
1.5	30.0	30.0	30.0	29.8	29.5	29.0
2.5	30.0	29.9	29.8	29.5	29.0	28.5
3.5	29.8	29.4	29.1	28.6	28.0	27.4
4.5	28.0	27.3	26.8	26.2	25.5	24.9
5.5	27.8	26.9	26.3	25.7	25.0	24.4
6.5	28.0	27.3	26.8	26.3	25.8	25.2
7.5	29.8	29.4	29.1	28.8	28.4	28.0
8.5	30.0	29.9	29.8	29.6	29.4	29.1
9.5	30.0	30.0	30.0	29.8	29.7	29.4

Table 4 Equivalent internal friction angle of the sand layer along the radius of soil with respect to the radius of disturbed zone (q=360 m^3/h)

Model cases	1	2	3	4	5	6
Jetting time, t	0.83h	2.33h	4.50h	7.50h	11.17h	15.67h
Radius of disturbed zone, $R(t)$	1.5 m	2.5 m	3.5 m	4.5 m	5.5 m	6.5 m
Radius of wet sand, Rs	Equivalent internal friction angle, φ' (deg)					
0.5	30.0	30.0	30.0	29.9	29.6	28.8
1.5	30.0	30.0	29.9	29.7	29.3	28.5
2.5	30.0	29.9	29.7	29.2	28.5	27.7
3.5	29.6	29.1	28.6	27.8	27.0	26.1
4.5	26.9	26.0	25.2	24.2	23.3	22.3
5.5	26.5	25.3	24.4	23.4	22.5	21.7
6.5	26.9	26.0	25.2	24.4	23.7	22.9
7.5	29.6	29.1	28.6	28.1	27.6	26.9
8.5	30.0	29.9	29.7	29.4	29.0	28.6
9.5	30.0	30.0	29.9	29.7	29.5	29.2

Table 5 Equivalent internal friction angle of the sand layer along the radius of soil with respect to the radius of disturbed zone (q=480 m^3/h)

Model cases	1	2	3	4	5	6
Jetting time, t	0.63h	1.75h	3.38h	5.63h	8.38h	11.75h
Radius of disturbed zone, $R(t)$	1.5 m	2.5 m	3.5 m	4.5 m	5.5 m	6.5 m
Radius of wet sand, Rs	Equivalent internal friction angle, φ' (deg)					
0.5	30.0	30.0	30.0	29.9	29.5	28.5
1.5	30.0	30.0	29.9	29.6	29.1	28.0
2.5	30.0	29.9	29.5	28.9	28.0	26.9
3.5	29.4	28.8	28.1	27.0	25.9	24.7
4.5	25.6	24.4	23.2	21.9	20.5	19.2
5.5	25.0	23.5	22.2	20.9	19.5	18.3
6.5	25.6	24.4	23.2	22.2	21.1	20.0
7.5	29.4	28.8	28.1	27.5	26.7	25.9
8.5	30.0	29.9	29.5	29.2	28.7	28.1
9.5	30.0	30.0	29.9	29.6	29.3	28.9

Tables 3-5 show the equivalent internal friction angle of the sand layer along the radius of soil with respect to the radius of disturbed zone and the water jetting flow rate respectively. The jetting times corresponding to each radius of disturbed zone with respect to the water jetting flow rate are shown in Fig. 4 and the change of equivalent internal friction angle of the sand layer when the radius of disturbed zone is 1.5 m and 6.5 m is respectively shown in Fig. 5.

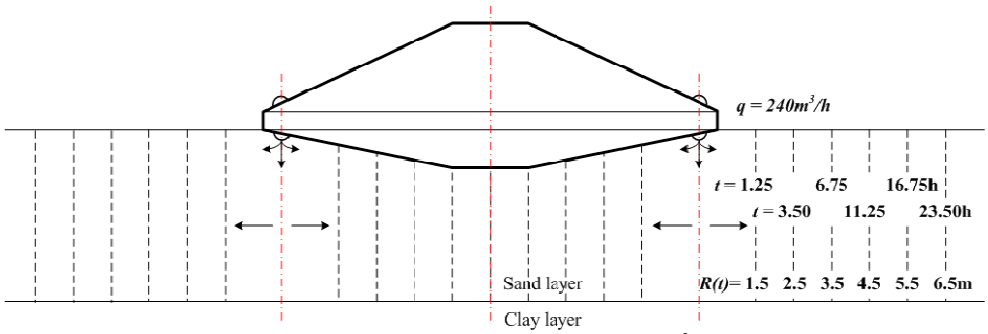

(a) when the jetting flow rate is 240 m^3/h

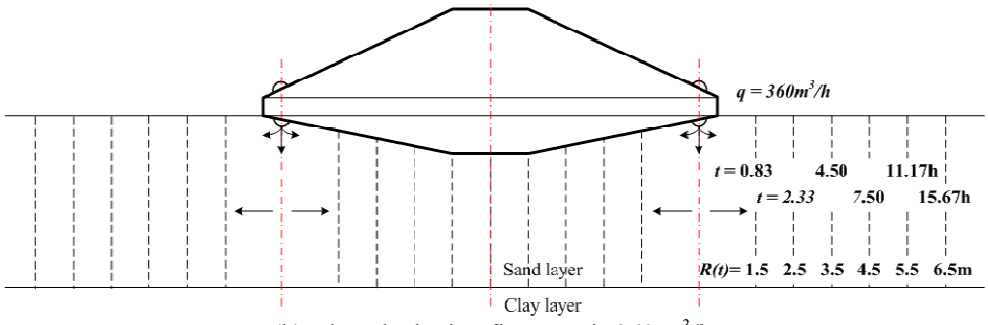

(b) when the jetting flow rate is 360 m^3/h

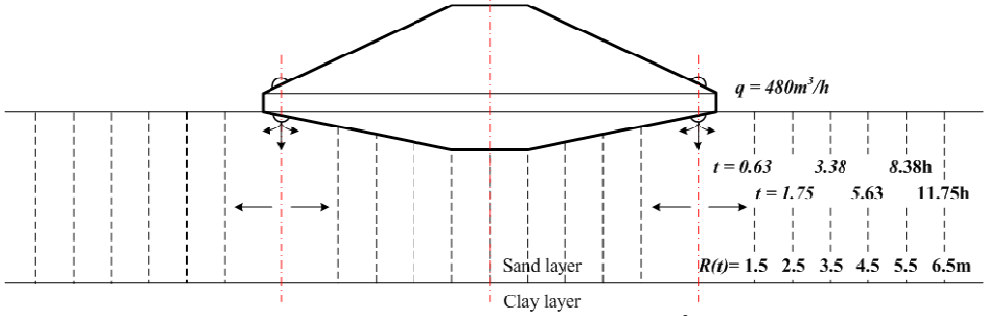

(c) when the jetting flow rate is 480 m^3/h

Fig. 4 Jetting time corresponding to each radius of disturbed zone with respect to the water jetting flow rate

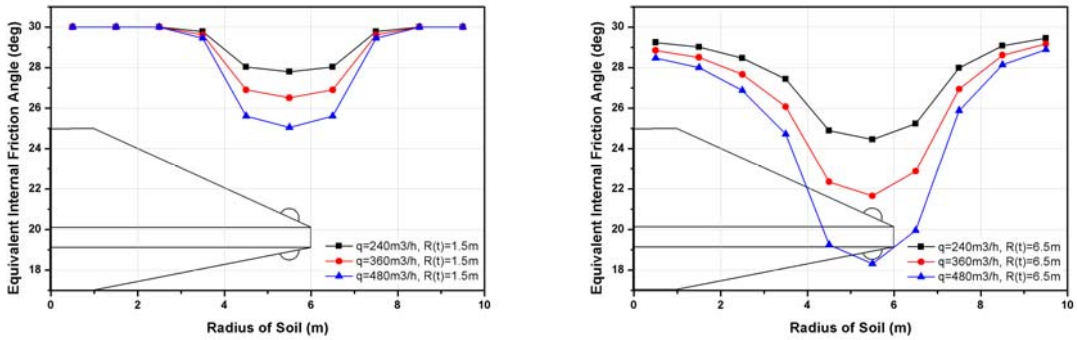

(a) $R(t)$ = 1.5 m (b) $R(t)$ = 6.5 m

Fig. 5 Equivalent internal friction angle of sand layer below each nozzle along the radius of soil with respect to the water jetting flow rate

4. Soil-Structure Interaction (SSI) analysis

4.1 Analytical/Numerical spudcan-soil model

Spudcan modeling The spudcan selected here consists of an approximated inverted cone with maximum diameter of 12.0 m, height of top to base 3.481 m, and the pitch circle radius of the jetting nozzles of 5.5 m. Its material is steel that behaves elastically. The jetting nozzles are located as close as possible to the outside of the spudcan, because the penetration depth critically depends on the shear resistance of a soil around the outside of the spudcan. Fig. 6 shows the schematics of the spudcan.

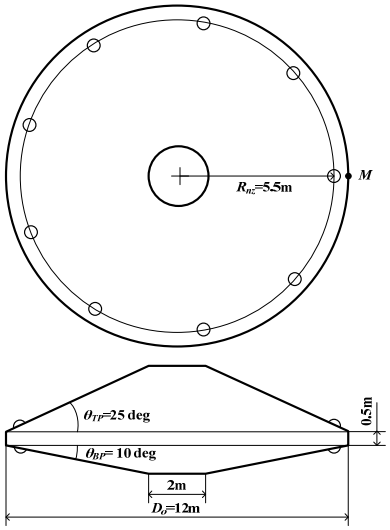

Fig. 6 Schematics of the spudcan

Table 6 Initial profile of soil

Soil type	Depth(*m*)	Submerged unit weight (kN/m^3)	Undrained shear strength (*kPa*)	Cohesion (*kPa*)	Internal friction angle (*deg*)
SAND	0 - 5.85	9.0	NA	10	30
CLAY(firm)	5.85 - 19.5	8.7	50	30	0
CLAY(stiff)	19.5 - 46.3	8.8	80	30	0

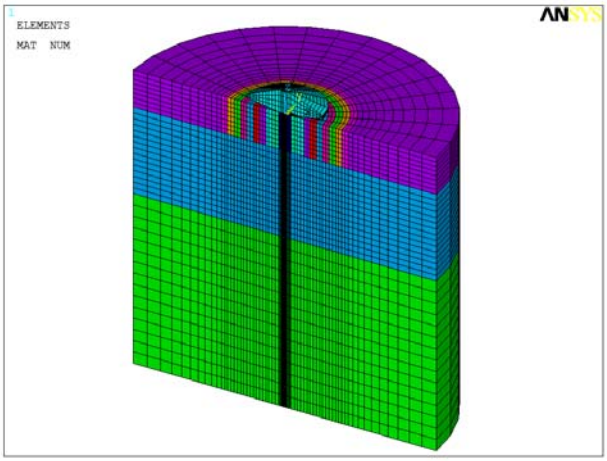

Fig. 7 Meshed shape and boundary condition for SSI analysis

Soil Modeling The initial profile of soil is given by Table 6. There are three soil layers (surficial sand and two clays below it) based on a specific site of GoM. The friction coefficient μ between the spudcan surface and soil is set up as 0.3. The Elastic modulus (E) is taken approximately $4\times q_c$ (for sand) and $200\times C_u$ (for clay), where q_c is the tip resistance from the CPT data and C_u is the undrained shear strength of clay. Poisson's ratios (ν) are 0.3 (for sand) and 0.49 (for clay), respectively. The dilatation angle (ψ) for sand is equal to the internal friction algle (φ) for the Mohr-Coulomb (MC) model. The Drucker-Prager (DP) model is derived from the MC model. In this study, Extended Drucker-Prager (EDP) model is used (Kai *et al*. 2009, Zhao *et al*. 2011).

Soil-structure interaction (SSI) modeling The soil-spudcan interaction is simulated by the surface-to-surface contact pair interaction. The spudcan is selected as a contact surface and the soil as a target surface. The friction coefficient is taken as 0.3 for the contact between sand and the spudcan. With water jetting, the friction coefficient may vary but the result is not that sensitive to its change. Radial directional d.o.f (ux) of nodes on the side surface of soil and vertical directional d.o.f (uy) of nodes on the bottom surface of soil are fixed, respectively. The vertical displacement (uy) of top of spudcan is pulled down to 3m vertically, after applying the acceleration of gravity. Fig. 7 shows the meshed shape and boundary condition for soil-spudcan interaction model (Kellezi

et al. 2003 and Qiu *et al*. 2012). In this study, the Soil-Structure Interaction (SSI) analysis is based on the implicit finite element method produced by ANSYS, for which only the Lagrangian (L) formulation is supported for a mesh solution. When the deformation is very large, the difference between the L formulation and Arbitrary Lagrangian-Eulerian (ALE) formulation may be increased, so if high accuracy is needed, ALE approach is preferred. However in this study, the spudcan penetration to the sand is typically small, so the results are to be reasonable for that purpose.

4.2 Results of SSI analysis

The soil-spudcan interaction analysis was carried out by using ANSYS program. The 3D model for the soil-spudcan is used as analysis option. Fig. 8 shows the equivalent plastic strain distribution of three layers of soil when the penetration depth is 3 m with respect to the water jetting flow rate.

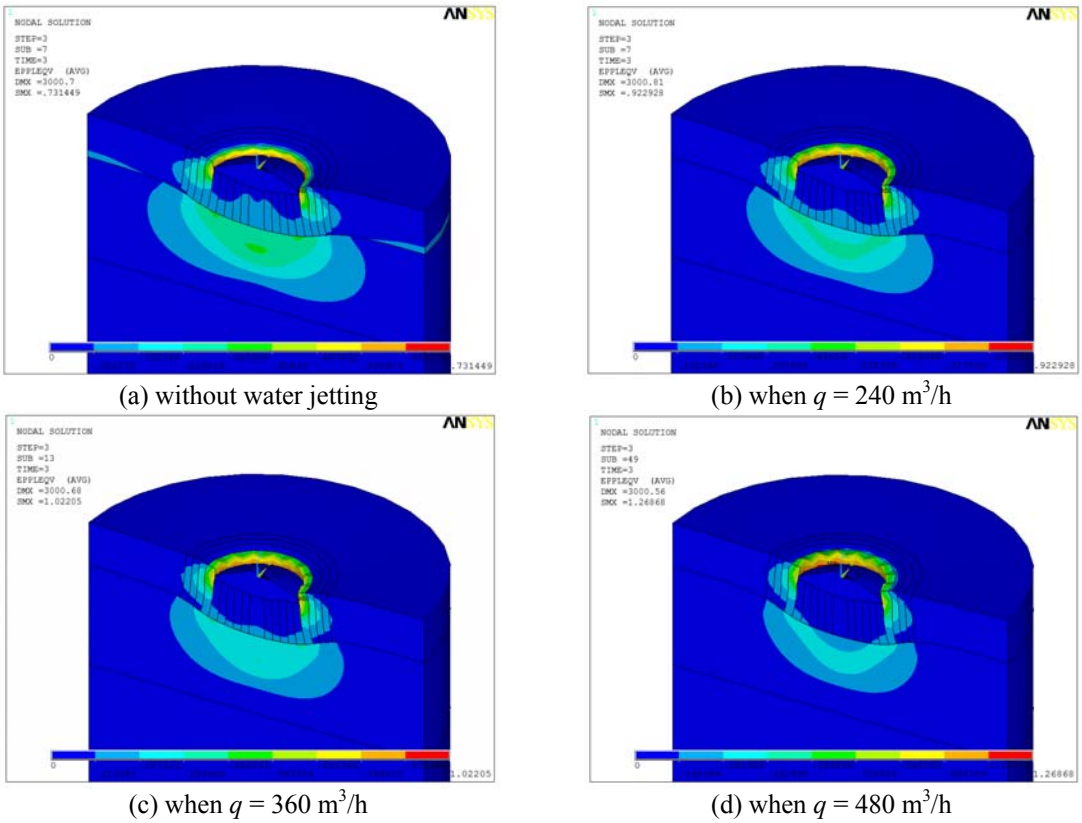

(a) without water jetting (b) when q = 240 m^3/h

(c) when q = 360 m^3/h (d) when q = 480 m^3/h

Fig. 8 Equivalent plastic strain distribution of soil when the penetration depth is 3m (when the radius of disturbed zone is 1.5 m)

Table 7 Peak resistance change with respect to the radius of disturbed zone and water jetting flow rate (q)

Radius of disturbed zone (m)	Peak resistance of soil (MN)		
	q=240 m^3/h	q=360 m^3/h	q=480 m^3/h
0.0 (without water jetting)	91.2	91.2	91.2
1.5	88.7	87.2	85.3
2.5	87.5	85.2	82.0
3.5	86.8	83.3	78.9
4.5	85.5	81.5	77.2
5.5	84.4	79.6	74.3
6.5	82.8	77.9	72.5

As shown in Fig. 8, shear failure occurs in the first layer (sand), the second layer (firm clay) is compressed, and the third layer (stiff clay) is little affected, while the spudcan penetrates the soil into 3 m-depth. The shear failure is easier in the first (sand) layer and the compressed region in the second (firm clay) layer is reduced, when the jetting flow rate is increased. Also, the equivalent plastic strain of the sand layer increases 1.26-, 1.40-, and 1.73-times compared to the model without water jetting respectively, when the jetting flow rate is 240, 360, and 480 m^3/h.

5. Results and discussions

5.1 Effect of the water jetting flow rate and time on the peak resistance of soil

To evaluate the effect of the jetting flow rate and time on the penetration resistance of a soil, the SSI analysis is carried out for 6-kinds of water jetting time corresponding to the radius of disturbed zone (1.5, 2.5, 3.5, 4.5, 5.5, 6.5 m) at 3-kinds of water jetting flow rate (240, 360, 480 m^3/h). Fig. 9 shows the penetration resistance of soil depending on the water jetting time at three water flow rates, respectively.

In Fig. 9, the initial smooth change in the penetration resistance is due to the compressive deformation of a soil below the spudcan, and the rapid drop is due to the shear failure/fracture of the first layer (sand) triggered at the spudcan side edge. The smooth curved part in the penetration resistance of the soil is little affected by water jetting and its flow rate but the peak resistance significantly decreases, as the water jetting flow rate and time increase.

To see the trend for the peak resistance change of soil in more detail after the water jetting, Table 7 shows its trend with respect to the radius of disturbed zone and water jetting flow rate. We can also see that with the increased flow rate, the spudcan can be lowered to the target depth more rapidly.

In Table 7, when the water jetting flow rate is 240 m^3/h, the penetration resistance of soil doesn't drop down below 80.45 MN even after 24-hours of water jetting time. Whereas, when the water jetting flow rate is 480 m^3/h, the penetration resistance can drop down below 80.45 MN

before 3-hours of water jetting time. The reduction rate of the peak resistance with water jetting to the model without water jetting is 9.2, 14.6, and 20.5%, respectively, when the radius of disturbed zone is 6.5 m.

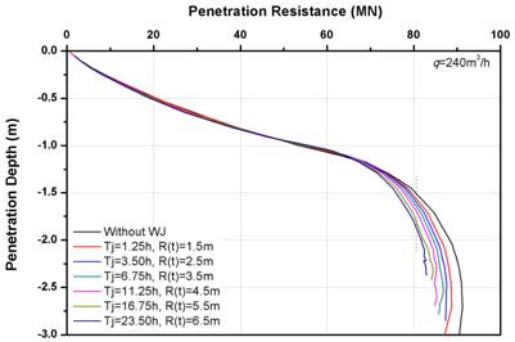

(a) when the jetting flow rate is 240 m^3/h

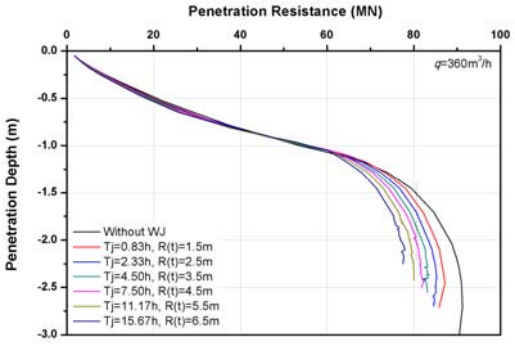

(b) when the jetting flow rate is 360 m^3/h

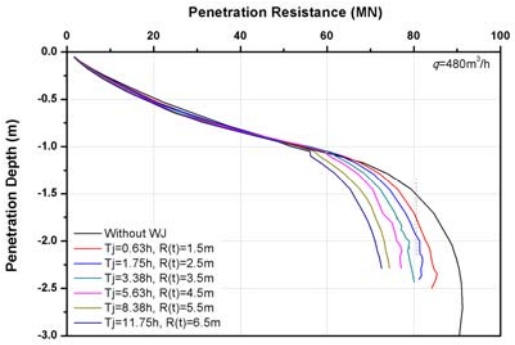

(c) when the jetting flow rate is 480 m^3/h

Fig. 9 Penetration resistance of soil according to the water jetting flow rate and time

Table 8 Water jetting time and penetration depth corresponding to the penetration resistance of 80.45MN with respect to the radius of disturbed zone and the water jetting flow rate (q)

Radius of disturbed zone (m)	q=240 m^3/h		q=360 m^3/h		q=480 m^3/h	
	Jetting time (*hour*)	Penetration depth (m)	Jetting time (*hour*)	Penetration depth (m)	Jetting time (*hour*)	Penetration depth (m)
0.0	0.00	-1.506	0.00	-1.506	0.00	-1.506
1.5	1.25	-1.559	0.83	-1.605	0.63	-1.745
2.5	3.50	-1.596	2.33	-1.697	1.75	-1.931
3.5	6.75	-1.635	4.50	-1.852	3.38	Punch-Through
4.5	11.25	-1.684	7.50	-2.001	5.63	Punch-Through
5.5	16.75	-1.792	11.17	Punch-Through	8.38	Punch-Through
6.5	23.50	-1.855	15.67	Punch-Through	11.75	Punch-Through

In case of surficial sand, this kind of shallow-penetration problem is well known to spudcan designers. The spudcan with outer diameter of 12 m can support the vertical loading of 80.45 MN (that is the maximum vertical loading applied on a spudcan) but the corresponding shallow penetration depths may not be enough to prevent overturning in harsh environments. Also, scour may cause additional problem. So, a water jetting system may be needed to insert the spudcan up to the required depth (over 1/2 of the height of a spudcan) to avoid those problems. Accordingly the penetration depth should be 1.74 m and more because the height of a spudcan is about 3.48 m.

5.2 Limit of water jetting flow rate and time in the surficial sand layer

To decide the proper water jetting flow rate and time to insert more than the 1/2 of spudcan height into the surfical sand layer, the water jetting time and the penetration depth corresponding to the applied vertical loading of 80.45 MN with respect to the radius of disturbed zone and the water jetting flow rate are shown in Table 8. Fig. 10 shows the penetration depth change with respect to the water jetting time and flow rate when the penetration resistance of 80.45 MN is reached. In Table 8, the punch-through case is defined when the peak reaction of soil cannot reach the applied vertical loading of 80.45 MN.

In Table 8, the penetration depth of the model without water jetting (initial condition) corresponding to the resistance of soil of 80.45 MN is 1.5 m. When the water jetting flow rate is 240 m^3/h, the penetration depth reaches to 1.855 m after the water jetting time of 23 h 30 m. When the water jetting flow rate is 360 m^3/h, the maximum penetration depth is 2.0 m for the water jetting time of 7 h 30 m. Similarly, when the water jetting flow rate is 480 m^3/h, the maximum penetration depth is 1.93 m for the water jetting time of 1 h 45 m. Also, if the penetration depth is greater than 2.0 m, the punch-through phenomenon occurs regardless of the water jetting flow rate. As shown in Fig. 10, the arrival jetting time to the 1/2 of spudcan height (1.74 m) is about 14.1 hours, 2.93 hours, and 0.62 hours, respectively, when the water jetting flow rate increases from

240 to 480 m^3/h. If the water jetting flow rate increases, the time to reach the target depth is shorter but the risk of punch-through is greater. Accordingly, it is important to decide the proper water jetting flow rate and duration according to the spudcan size, shape, and the soil condition. The principal purpose of using the water jetting in surficial sand condition is to insert the spudcan up to the required depth. In this regard, the water jetting flow rate and duration should be selected to minimize the time while not exposing to the risk of punch-through failure.

5.3 Effect of the jetting flow rate and time on the overturning moment and the shear loading

The water-jetting may also reduce the structure-soil resistance against shear loading and overturning moment. To see the effect, the overturning and the horizontal resistance of a soil according to the water jetting flow rate are analyzed when the vertical penetration resistance of 80.45MN and the penetration depth is 1/2 of spudcan height (1.74 m). Fig. 11 shows the equivalent plastic strain of a soil with changing jetting flow rate when the overturning moment and horizontal shear loading of Table 2 are respectively applied on the spudcan when the penetration resistance is reached at 80.45 MN. We can see more strain at higher flow rate that results in weaker resistance against shear and overturning loadings. Fig. 12 shows the change of overturning and horizontal resistance of the soil according to the water jetting flow rate when the vertical resistance of a soil is 80.45 MN.

In Fig. 12, all the cases can sufficiently resist the present maximum shear forces 2.78 MN and maximum overturning moment 103.1MN-m (see Table 2) when the penetration depth is 1/2 of spudcan height (1.74 m). In general, the resistance capability of a soil with water jetting against shear and moment loadings decreases compared with that without water jetting but the resistance capability of a soil is still acceptable regardless of the jetting flow rate if the penetration resistance is 80.45 MN at the penetration depth of 1.74 m. Accordingly, the resistance against such loadings is sufficient regardless of water-jetting flow rate when the target penetration depth is achieved.

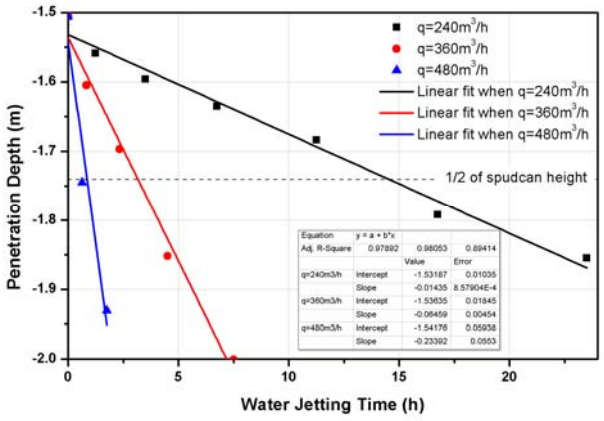

Fig. 10 Penetration depth change of a spudcan with respect to the water jetting time and flow rate when the penetration resistance is 80.45 MN

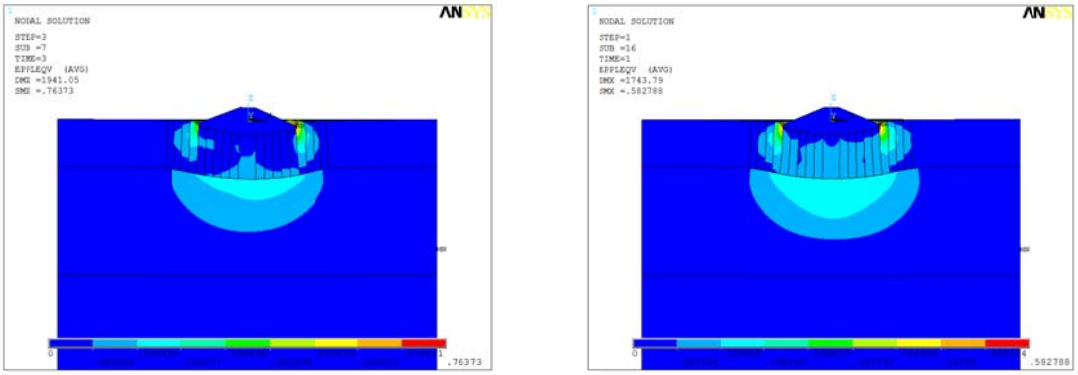

(a) when the jetting flow rate is 240 m^3/h

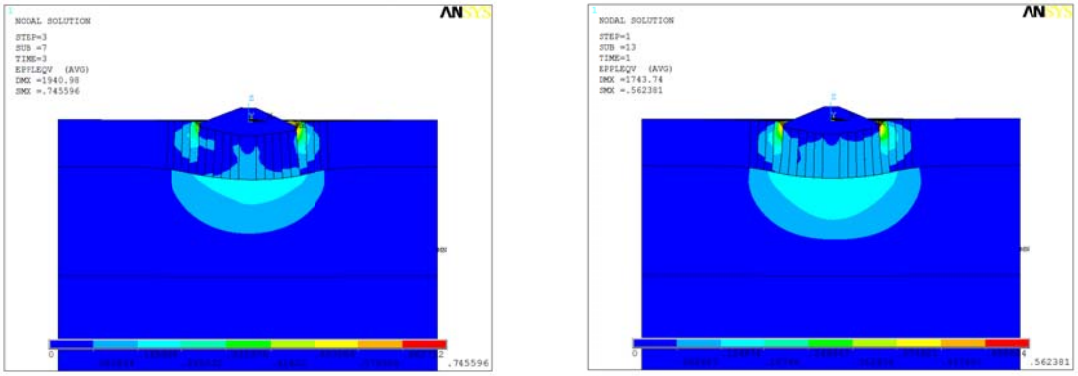

(b) when the jetting flow rate is 360 m^3/h

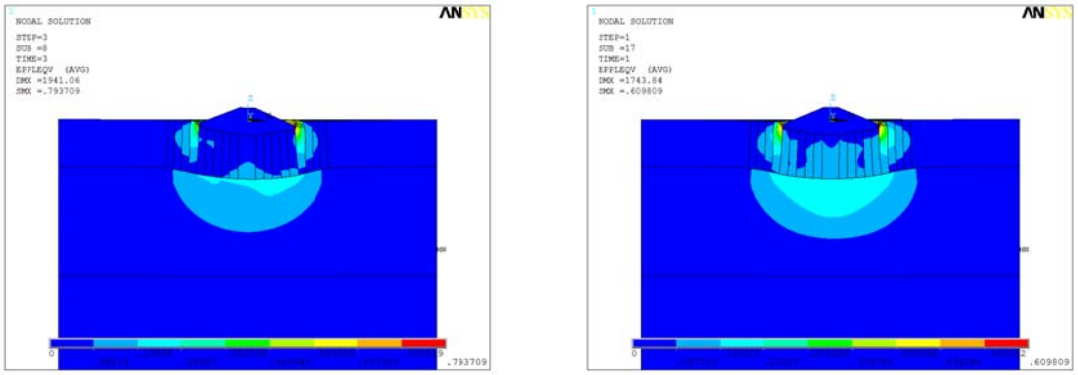

(c) when the jetting flow rate is 480 m^3/h

Fig. 11 Equivalent plastic strain distribution of a soil for the overturning moment (left figure) and the horizontal shear loading (right figure) according to the jetting flow rate when the vertical resistance of soil is 80.45 MN

6. Conclusions

In this study, soil-spudcan interaction analysis is carried out to evaluate the effect of water jetting flow rate and time on the penetration resistance in the surficial sand condition overlaying two clay layers. In this regard, the sample spudcan with outer diameter of 12 m, designed for a sample jack-up rig of weight (maximum vertical loading applied on each leg is 80.45 MN) is numerically modeled for the required depth of 1.74 m (minimum 1/2 of spudcan height). Since the target penetration depth cannot be reached without water jetting, water jetting is needed to insert the spudcan up to the sufficient depth. The equivalent internal friction angle decreases up to 24.5°, 21.7°, 18.3° from initial 30° when the water jetting flow rate increases from 240 m^3/h to 480 m^3/h. The rate of change also depends on the special distance from each nozzle. In particular, the equivalent internal friction angle is significantly reduced within the radius of 1m from the jetting nozzle. The peak resistance of soil for the model without water jetting is 91.2 MN. The peak resistance of soil with water jetting can be reduced by 9.2% ~ 20.5% compared to the case without water jetting when the water jetting flow rate increases from 240 m^3/h to 480 m^3/h. The jetting time to reach the target depth (1.74 m) is about 14.1 hours, 2.93 hours, and 0.62 hours, respectively, with increasing flow rate from 240 to 480 m^3/h. Also, the resistance against external and gravitational loadings is sufficient regardless of water-jetting when the penetration depth is 1/2 of spudcan height. However, if the penetration depth is greater than 2.0 m, the punch-through phenomenon starts to occur regardless of the water jetting flow rate. Also, if the water jetting flow rate increases, the jetting time for the target penetration depth becomes shorter but the risk of punch-through is greater. The present case study assumed constant water jetting flow rate with time but it can be straightforwardly extended to time-dependent variable flow rate cases. This kind of numerical simulation is necessary to better understand the overall physics and develop an optimal smart-spudcan operation with flow rate control in the future.

Acknowledgements

This research was supported by the Innopolis Busan under the R&D program supervised by the Korea Ministry of Science, ICT and Future Planning.

References

American Petroleum Institute (2007), *API BULLETIN 2INT-MET Interim guidance on hurricane conditions in the Gulf of Mexico*, Washington, D.C., U.S.A.

ANSYS, Inc., 2012. *ANSYS Mechanical APDL Material Reference*, 47-57.

Det Norske Veritas AS (2012), *Self-elevating Units*.

Duan, M., Zhao, J., Wang, J. and Song, L. (2013), "Jetting effect of jackup on actively punching through overlaid sand layer", *Int. J. Offshore Polar.*, **23**(1), 55-62.

Kai, S.U. and Yin, L.I. (2009), "Discussion of extended Drucker-Prager yield criterion in slope stability analysis", *Proceeding of the Power and Energy Engineering Conference*, 2009 APPEEC.

Kang, H.Y. and Kim, M.H. (2012), "Hydrodynamic interactions and coupled dynamics between a container ship and multiple mobile harbors", *Ocean Syst. Eng.*, **2**(3), 217-228.

Kim, M.H. and Chen, W. (1994), "Slender body approximation for slowly-varying wave loads in multi-directional waves", *J. Appl. Ocean Res.*, **16**(3), 141-163.

Kim, M.H. and Ran, Z. (1994), "Responses of an articulated tower in waves and currents", *Int. J. Offshore Polar*, **4**(4), 298-391.
Kellezi, L. and Stromann, H. (2003), "FEM analysis of jack-up spudcan penetration for multi-layered critical soil conditions", *Proceeding of the BGA International Conference on Foundations*.
Han, D.S., Kim, S.J. and Kim, M.H. (2014), "Effect of plate slope and water jetting on the penetration depth of a jack-up spud-can for surficial sand", *Ocean Syst. Eng.*, **4**(4), 263-278.
Han, D.S., Kim, S.J., Kim, M.H. and Park, Y.C. (2014), "Relation between slope of plate and reaction of soil in a spudcan for jack-up platform", *Proceeding of the International Offshore and Polar Engineering Conference*, 2014 ISOPE.
Qiu, G. and Grabe, J. (2012), "Numerical investigation of bearing capacity due to spudcan penetration in sand overlying clay", *Can. Geotech. J.*, **49**, 1393-1407.
Tho, K.K., Leung, C.F., Chow, Y.K. and Swaddiwudhipong, S. (2012), "Eulerian finite-element technique for analysis of jack-up spudcan penetration", *Int. J. Geomech. - ASCE*, **12**(1), 64-73.
Yang, C.K. and Kim, M.H. (2011), "The structural safety assessment of a tie-down system on a tension leg platform during hurricane events", *Ocean Syst. Eng.*, **1**(4), 263-283.
Yu, L., Hu, Y., Liu, J., Randolph F.M. and Kong, X. (2012), "Numerical study of spudcan penetration in loose sand overlying clay", *J. Comput. Geotech.*, **46**, 1-12.
Zhao, J., Duan, M., Cao, S., Hu, Z. and Song, L. (2011), "Prediction of spudcan penetration depth in multiple layers with sand overlying clay", *J. Appl. Mech. Mater.*, **52-54**, 995-1002.